Regional climate projections of daily extreme temperatures in Argentina applying statistical downscaling to CMIP5 and CMIP6 models

Rocio Balmaceda-Huarte

rbalmaceda@at.fcen.uba.ar

Universidad de Buenos Aires https://orcid.org/0000-0003-2188-2797

Matias Ezequiel Olmo

Barcelona Supercomputing Center: Centro Nacional de Supercomputacion

Maria Laura Bettolli

Universidad de Buenos Aires Facultad de Ciencias Exactas y Naturales

Research Article

Keywords: Extreme temperatures, global climate models, daily temperature, climate change, statistical downscaling, regional climate models

Posted Date: November 7th, 2023

DOI: https://doi.org/10.21203/rs.3.rs-3492471/v1

Version of Record: A version of this preprint was published at Climate Dynamics on March 4th, 2024. See the published version at https://doi.org/10.1007/s00382-024-07147-9.

Abstract

Argentina is a wide country with a variety of climates, where an increase in mean and extreme temperatures is currently on-going, demanding regional climate information to design and implement effective strategies for climate change adaptation. In this regard, the use of Empirical Statistical Downscaling (ESD) procedures can help providing tailored climate information. In this work, a set of ESD models were tested to generate plausible regional climate projections for daily maximum and minimum temperatures (Tx, Tn) in Argentina. ESD models were applied to an ensemble of CMIP5 and CMIP6 global circulation models (GCMs) to downscale historical and future worst-case scenarios. The plausibility of the ESD projections was analysed by comparing them with their driving GCMs and with CORDEX regional climate models (RCMs).

Generally, all ESD models added value during the historical period, in mean values as well as in extreme indices, especially for Tx. The climate projections depicted an extended signal of warming (both in the mean and in the frequency of extremes), consistent between all simulations (GCMs, RCMs and ESD) and strongest over northern Argentina. ESD models showed potential to produce plausible projections, although, depending on the technique considered (for Tx) and the predictor configurations (for Tn), differences in the change rates were identified. Nevertheless, the uncertainty in future changes was considerably reduced by RCMs and ESD when compared to their driving GCMs.

Overall, this study evidences the potential of ESD in a climate change context and contributes to the assessment of the uncertainty on the future Argentine climate.

1. Introduction

Climate change has led to an increase in global temperature that will, with high confidence, continue during the upcoming years modifying different aspects of the climate system (Almazroui et al. 2021; Gulizia et al. 2022; Collazo et al. 2022; De Luca and Donat 2023, Avila-Diaz et al. 2023; Engdaw et al. 2023; Alexander and Arblaster, 2017). However, assessing the differentiated patterns and rates of change in a regional scale is of utmost importance to set up well-informed policy strategies of adaptation and mitigation of the observed and future local changes (IPCC 2021). In this regard, Argentina (located in the southern tip of South America, roughly between 55–75 °W and 20–60 °S) is a wide country with different climatic regions, where an increase in mean temperature has been detected as well as an amplification of temperature extremes including heatwaves duration and intensity (Rusticucci et al. 2016; Olmo et al. 2020; Suli et al. 2023; Coronato et al. 2023). Furthermore, this sort of climate hazards have a strong impact on different socio-economic activities, energy production and distribution, and also on human health, increasing stress conditions and mortality particularly of the most vulnerable age ranges (Almeira et al. 2016; Fontan and Rusticucci 2021; Miranda et al. 2023).

Within the scientific community, the use of global climate models (GCMs) is one of the most valuable tools when performing studies of observed and future climate variability and change. They are

consistently organised and freely distributed within different versions of the *Coupled Model Intercomparison Project* (CMIP). These simulations provide outputs of several climatic variables in multiple time-steps, numerically resolving the system of equations that govern the atmosphere and parametrizing some physical processes and mechanisms that can not yet be explicitly resolved due to still unknown mechanisms and not enough resolution (Ambrizzi et al 2018, Taylor et al. 2012; Eyring et al. 2016). Hence, different methods of downscaling are available to obtain from the GCMs regional climate information at a finer scale. Empirical statistical downscaling (ESD) arises as a promising and competitive procedure based on the observed link between the large-scale and surface atmospheric variables (Maraun et al. 2010), with a significantly reduced computational cost than dynamical downscaling, another popular strategy based on regional climate models (RCMs), like the ones put in line within the initiative *Coordinated Regional Climate Downscaling Experiment* (CORDEX). Both approaches have their different strengths and limitations, but have demonstrated added value in their representation of the local climate in different regions of the world (Huth et al. 2015; Casanueva et al. 2016; Gutiérrez et al. 2019; Olmo et al. 2022a; Balmaceda-Huarte et al. 2023). In particular, different efforts have been made for ESD experiments over southern South America (SSA) employing a variety of statistical methods including analogs, regressions and clustering procedures (D'onofrio et al. 2010; Bettolli and Penalba 2018; Araya-Osses et al. 2021; Mutz et al. 2021). More recently, in some areas of SSA, focus has been put especially on extreme precipitation (Bettolli et al. 2021; Solman et al. 2021; Olmo et al. 2022b). These studies highlighted the potential of different downscaling tools to represent complex phenomena like heavy rainfall, that GCMs struggle to simulate due to misrepresentation of its leading mechanisms. Whereas statistical downscaling of daily maximum and minimum temperatures (Tx and Tn, respectively) has been evaluated in a previous work by Balmaceda-Huarte and Bettolli (2022), where a set of analogs, generalised linear models and artificial neural networks were employed. The authors found, during an observed period using a cross-validation approach, a good performance of the models, being successful to reproduce the mean values, extreme percentiles and temporal variability from seasonal to interannual. Moreover, these models were able to simulate a particular validation set of warmer years, indicating their potential to be used for climate change studies. However, only few studies assessed the evaluation of future projections of extreme temperatures on a regional scale, based on RCM outputs (Carril et al. 2016; López Franca et al. 2016; Lagos-Zuñiga et al. 2022; Reboita et al. 2022; Olmo et al. 2022b; Blázquez and Solman 2023). In particular, the use of ESD ensembles is still incipient over the region (Araya-Osses et al. 2021; Mutz et al. 2021) and has not been carried out for producing detailed Tx and Tn climate projections over Argentina so far.

Thus, the generation of future climate projections of daily extreme temperatures by means of ESD strategies is still an open line of research over Argentina that could help ascertain our confidence in a global warming scenario.

In this context, the aim of the present work is to analyse the suitability of a multi-model ensemble of statistically downscaled GCMs to generate plausible regional climate projections for Tx and Tn in different climatic regions of Argentina. To do so, a set of ESD models previously evaluated in Balmaceda-Huarte and Bettolli (2022) and found with the best skills within the calibration and validation experiment

will be used to downscale a set of CMIP5 and CMIP6 GCMs to build an ESD ensemble for the 21st century. Moreover, the plausibility of these projections will be analysed by comparing them with their driving GCMs outputs and the available CORDEX RCM simulations over Argentina. This paper is structured as follows: Section 2 presents the observational and model data employed here, Section 3 describes the ESD experiment; Section 4 shows the results of the application of the ESD models into the GCMs in their historical period and the climate change projections, including the intercomparison with RCM outputs and, lastly, Section 5 presents a discussion and some final remarks of this study.

2. Data

Station data

Daily maximum and minimum temperature (Tx and Tn) observed at 101 meteorological stations of Argentina were considered during the period 1979–2018 (Fig. 1). The station network presented less than 10% of missing information in the total period and has been previously used and quality-controlled in Balmaceda-Huarte and Bettolli (2022). All station data was provided by the National Weather Service of Argentina.

Since Argentina is a wide country that comprises a variety of climates (Beck et al. 2018), to better represent their different characteristics the total domain was divided into five subregions. The regions considered were the Pampas region (R1), northeast Argentina (R2), central Argentina (R3), northwest Argentina (R4) and Argentinian Patagonia (R5) (Fig. 1) following Balmaceda-Huarte and Bettolli (2022).

Gridded data: Reanalysis, GCMs and RCMs

Daily fields from the ECMWF ERA-Interim reanalysis (ERA, Dee et al. 2011) were used as large scale predictors to train the ESD models in the period 1979–2018. The variables considered for the different ESD models were meridional and zonal wind at 1000 hPa (v1000 and u1000), air temperature and specific humidity at 850 hPa (T850 and q850) and sea level pressure (slp). The predictors domain extends between 14–58 °S and 44–80 °W (Fig. 1) and encloses Argentina, part of the Pacific and Atlantic oceans and the Andes mountain range, key features of the southern South America atmospheric circulation (Barros et al. 2002; Bettolli and Penalba, 2018; Balmaceda-Huarte and Bettolli, 2022).

Daily outputs from 14 GCMs from the CMIP5 and CMIP6 modelling experiment (Taylor et al. 2012; Eyring et al. 2016) listed in Table 1 were used in the application of the ESD models. The selection of the GCMs was made according to the data availability of the chosen predictor variables in the domain (Fig. 1) since some GCMs exhibited missing data near the complex topography of the Andes mountain range. For both experiments, historical and future simulations from the worst-case scenario were employed. In the case of CMIP5 (CMIP6) models the evaluation of historical simulations was done in the period 1979–2005 (1979–2014) and the RCP8.5 (SSP585) future scenario in the period 2006–2100 (2014–2100). In particular, the MPI-ESM1-2-LR CMIP6 model (Table 1) was not employed for the analysis of future projections due to some outliers in the v1000 predictor data during the period 2071–2100.

Large scale predictors from ERA and all GCMs were re-gridded using bilinear interpolation and taken to a common 2º spatial grid resolution to ease the intercomparison. In all cases, standardised anomalies of the predictor variables (by gridbox) were used as input for the ESD models.

Additionally, daily Tx and Tn raw outputs (RAW) from the GCMs (Table 1) were considered, selecting the closest grid cell –keeping the GCM native resolution– to the meteorological station point (Fig. 1).

Finally, in order to intercompare dynamical and statistical downscaling future simulations, daily Tx and Tn from three different regional climate models (RCMs) contributing to the CORDEX initiative (Giorgi et al., 2009; Jones et al. 2011) were taken into account (Table 2). In particular, the simulations of RegCM4.7 and REMO2015 models (Table 2) belonging to the CORDEX-CORE experiment (Gutowski et al., 2016) and the Eta model (Chou et al. 2004) were used. These simulations are nested by three different GCMs of CMIP5 (Table 2), which cover the historical period (1981–2005) and climate change projections for the period 2006–2099 in the RCP8.5 scenario. Although all ESD simulations were performed for all GCMs in Table 1, for the comparison with RCMs, only ESD simulations using the three GCMs forcing the RCMs were considered.

Similar to the GCMs RAW outputs, the closest grid cell from each RCMs native grid to the meteorological station point was considered. The Eta model (Chou et al. 2014) domain did not cover all Argentina, in this case only the station points included in the Eta domain were considered.

Table 1
Global Climate Models (GCMs) used in this study.

Experiment	*Model*	*Reference*	*Resolution*	*Variant Lebel*
CMIP5	CanESM2	Kirchmeier-Younget al. (2017*)*	2.8° × 2.8°	r1i1p1
	CMCC-CESM	*Hurrell et al. (2013)*	3.7° × 3.4°	r1i1p1
	CMCC-CM	*Scoccimarro et al. (2011)*	0.7° × 0.7°	r1i1p1
	CMCC-CMS	Weare et al. (2012)	1.9° × 1.9°	r1i1p1
	CNRM-CM5	*Voldoire et al. (2013)*	1.4° × 1.4°	r1i1p1
	EC-Earth	*Hazeleger et al. (2010)*	1.12° x 1.12°	r12i1p1
	MPI-ESM-LR	*Giorgetta et al. (2013)*	1.9° × 1.9°	r1i1p1
	MPI-ESM-MR	*Giorgetta et al. (2013)*	1.9° × 1.9°	r1i1p1
	NorESM1-M	*Bentsen et al. (2013)*	1.9° × 2.5°	r1i1p1
CMIP6	CanESM5	*Swart et al. (2019)*	2.8° × 2.8°	r1i1p2f1
	MPI-ESM2-1-HR	*Mueller et al. (2018)*	0.9° × 0.9°	r1i1p1f1
	MPI-ESM2-1-LR	*Mueller et al. (2018)*	1.9°×1.9°	r1i1p1f1
	NorESM2-LM	*Bentsen et al. (2013)*	1.9° x 2.25°	r1i1p1f1
	NorESM2-MM	*Bentsen et al. (2013)*	0.9° × 1.25°	r1i1p1f1

3. Methodology

ESD models

Following the assessment carried out in Balmaceda-Huarte and Bettolli (2022), a subset of ESD models were selected for this study (Table 3). This selection took into account three different ESD techniques: analogs (ANs), generalised linear models (GLMs) and artificial neural networks (ANNs); and two predictor combinations (P1 and P2) with three different configurations (point-wise and spatial-wise predictors, and combination of both). Predictors set P2 and P1 include variables representative of the atmospheric circulation, temperature and humidity (see Table 3) and also informative of the climate change signal, in agreement with climate change ESD studies over the region (Mutz et al. 2021; Araya-Osses et al. 2020). Regarding predictor configurations, in the point-wise predictors the four nearest grid points (L) to the target station point were considered, while for the spatial predictors (S), the whole domain were used (pink box in Fig. 1) and empirical orthogonal functions (EOFs) were applied to reduce dimensionality and co-linearity. Both approaches were combined in local-spatial-wise (LS). Predictor configuration and the way the ESD models were constructed are further explained in a previous work (Balmaceda-Huarte and Bettolli, 2022).

All ESD models from Table 3 were trained separately at each meteorological station (single-site approach). A brief description of the methods considered for this study are described below.

Table 2
Regional Climate Models (RCMs) used in this study.

RCM	*Driving GCM*	*Reference*	*Resolution*
Eta	CanESM2	*Chou et al. (2014)*	0.20°
RegCM4-7	MPI-ESM-LR NorESM1-M	*Giorgi et al. (2012)*	0.22°
REMO2015	MPI-ESM-MR NorESM1-M	*Jacob et al. (2012)*	0.22°

The *AN* technique described by Zorita and von Storch (1999) was employed. This method looks for similarities -using the Euclidean norm- between the daily large-scale predictors from ERA and the GCMs. From this procedure, an analog day is identified for each day of the GCMs, and the corresponding value from the observation record is used for prediction (Horton 2021, Araya-Osses et al. 2020, Gutierrez et al. 2013). In this sense, the AN method is restricted to the situations observed during the period of training (1979–2018).

Table 3
Predictors and configurations selected for the three methods ANs, GLMs, and ANNs. L(S) indicates the local (spatial) configuration of the predictor.

Predictors	*Configuration*	*Label*
P1: u1000, v1000, T850 and q850	L (u1000 + v1000 + T850 + q850)	P2.L
	S (u1000 + v1000 + T850) + L (q850)	P2.LS
	S (u1000 + v1000 + T850 + q850)	P2.S
P2: T850, q850 and slp	S (T850 + slp) + L (q850)	P1.LS.a

The *ANN* models are essentially non-linear regressions composed of three types of layers: an input layer (predictors information), an output layer (observations) and one or more hidden layers in between. Several neurons are grouped in these layers, which are fully connected by weights and output signals. These output signals are obtained from the sum of the inputs to the neurons modified by an activation function (Gardner and Dorling, 1998). For this work, the ANNs architecture tested in Balmaceda-Huarte and Bettolli (2022) was employed with two-layers of 25 and 15 neurons, respectively. Also, the sigmoid and linear activation functions were considered in the hidden and output layers, respectively. Furthermore, the different weights were optimised during the calibration process using the backpropagation algorithm (Rumelhart et al. 1986; Hernanz et al. 2021; Wang et al. 2021) and the mean squared error as cost function, setting the learning rate parameter to 0.01 and a batch size of 100.

In the case of daily temperatures —which can be sensibly modelled by a normal distribution— the GLMs models are equal to a multiple linear regression (Maraun and Witmann, 2018). In these models, the link between the predictor (large-scale variables) and the predictand (Tx and Tn observed) is approximate via some linear function whose coefficients are defined in the training phase (Huth, 1999; Asong et al., 2016). Despite its simplicity, GLM models have been widely used to downscale temperature especially as a benchmark method to evaluated brand-new techniques (Fan et al. 2021, Hernanz et al. 2021, Baño-Medina et al. 2021).

Perfect prognosis assumption

Under the perfect prognosis approach (PP), the ESD models are trained considering “perfect” conditions, taking predictand data from meteorological stations and large-scale predictors from reanalysis (which are considered as pseudo-observations); and then applied to the GCMs predictor data under the assumption that predictors are well simulated by the GCMs —perfect prognosis assumption—. However, GCMs are usually “not perfect” and biased with respect to the reanalysis data (Balmaceda-Huarte et al. 2023). Thus, to alleviate the mismatch between ERA and the GCMs and fulfil the perfect prognosis assumption, GCMs predictor data were bias-corrected as in Baño-Medina et al. (2022) and Balmaceda-Huarte et al. (2023). In this regard, the GCMs predictor data were adjusted in mean and variance on a monthly basis to the ERA predictors used for training. To preserve trends, this procedure was done in two steps: first the historical period was corrected; and second, the future scenario, in which the delta change signal was previously removed and then added to the corrected predictors. Note that this correction minimises the potential errors that may appear in the future downscaled scenarios and therefore circumvent on implausible future projections (Baño-Medina et al. 2022; Manzanas et al., 2020; Vrac and Ayar, 2016).

Historical and future scenarios

Tx and Tn downscaled series from the different GCMs were first evaluated during the historical period taking the station observations as reference. The seasonal mean values in terms of bias were assessed considering days from austral summer (DFJ) for Tx and winter (JJA) for Tn. These calculations were done for the historical period of CMIP5 and CMIP6, respectively.

Further evaluations were done in a common reference period 1986–2005. Following the framework of the VALUE experiment over Europe (Maraun et al. 2015; Hertig et al. 2017), several validation indices described in Table 4 were estimated addressing marginal and temporal aspects of the ESD models simulations. All the indices were calculated for each station —or the closest grid cell to the station point, in the case of the RAW model outputs— and then regionally aggregated.

Future projections were analysed with respect to the reference period by means of delta changes: differences between the mean values of the far future (1971–2100) and the reference period were calculated for each Tx and Tn ESD simulation from both future scenarios (RCP8.5 and SSP85)

independently. To intercompare the far-future signal, the delta change was computed for both the RAW GCM outputs and RCMs simulations.

Finally, average regional time-series during the complete period of study (1979–2100) were constructed by merging the historical and future scenarios. With the aim of analysing extreme aspects of the future projections, the temporal evolution of the indices cold and hot days detailed in Table 4 and two percentile-based indices from the ETCCDI (Klein Tank et al. 2009) (Table 4) were analysed.

All calculations implemented in this study were performed using the R-based *climate4R* open framework (Iturbide et al. 2019; Bedia et al. 2020).

4. Results

4.1 Historical scenario

a Seasonal biases

As an initial evaluation the ensamble mean of the ESD simulations in the historical period was explored. The spatial distribution of the bias for the warmest (Tx during summer) and coldest (Tn during winter) temperatures of the year are displayed in Fig. 2 considering the ensemble mean of CMIP5 and CMIP6 simulations for each ESD and RAW outputs. Results

Table 4
Indices analysed in this study. P90 (P10) refers to the 90th (10th) percentile calculated during the reference period 1986–2005.

Index	*Temporal scale*	*Descriptions*	*Variable*	*Unit*
AnnualCycleAmp	*Annual*	Amplitude of the annual cycle	Tx ,Tn	°C
P98	*DFJ*	98th percentile	Tx	°C
P02	JJA	2th percentile	Tn	°C
Hot days	Annual	Number of days in the year with Tx > 30°C	Tx	days
Cold days	Annual	Number of days in the year with Tn < 0°C	Tn	days
ColdAnnualMaxSpell	Annual	Median of the annual cold (Tn < P10) spell maxima	Tn	days
WarmAnnualMaxSpell	Annual	Median of the annual warm (Tx > P90) spell maxima	Tx	days
Tx90p	Annual	Number of days in the year with Tx > P90	Tx	days
Tn90p	Annual	Number of days in the year with Tn > P90	Tn	days

showed that ESD simulations considerably reduce the biases observed in the RAW outputs for both experiments (CMIP5 and CMIP6) and variables. This was more clear for Tx than Tn, for which RAW ensembles showed larger errors. For both temperatures, similar patterns of biases were exhibited in CMIP5 and CMIP6 RAW ensembles. Summer Tx was highly underestimated along the Andes Mountain range (R4) and in Patagonia region (R5) while overestimated in northeastern Argentina (R1 and R2). The coldest temperatures were mostly overestimated by the RAW ensembles with the exception of the stations near the Andes Mountain range (R4).

Regarding the ESD simulations, generally, cold (warm) biases for Tx (Tn) were observed, slightly higher for Tn (Fig. 2). No clear distinctions were detected between the CMIP5 and CMIP6 ensembles, which performed similarly despite the imbalance in the number of GCMs included in each ensemble. However, some differences were highlighted among the ESD models performance. The AN model that considered only local information of the predictors (AN.P2.L) exhibited the largest differences with the observations in all stations for both predictand variables. This characteristic of the models with local predictor configuration was also observed in the GLM and ANN families, where GLM.P2.L and ANN.P2.L presented coldest (warmest) biases for Tx (Tn) than the rest of the configurations. Nevertheless, these biases (with

the exception of the AN.P2.L, in some stations) did not exceed 1ºC in absolute values, and stayed close to the errors obtained during cross-validation on an annual basis (Balmaceda-Huarte and Bettolli, 2022).

b Indices

A deeper inspection of the ESD simulations was carried out in the period 1986–2005 by analysing multiple indices. Results are summarised in boxplots in Figs. 3 and 4 for Tx and Tn, respectively. Boxplot displays: the observed value of the indices at each station point for each region; the indices estimation for each ESD model and RAW simulation regionally averaged for each GCM expressed in terms of bias. Regarding Tx (Fig. 3), the amplitude of the annual cycle (AnnualCycleAmp) of the different regions was well captured by the downscaled simulations. Exceptionally, the AN.P2.L highly underestimated the observed values, specially in R5 (Patagonia Argentina) —region with the largest annual amplitude (Fig. 3a)—. This result for the AN.P2.L was in line with the biases detected in Fig. 2, and also to a strong overestimation of the winter Tx by the analog method, that was already identified when the ESD models where forced with reanalysis data (Balmaceda-Huarte and Bettolli, 2022). For the rest of the ESD models, underestimations of the annual cycle amplitude were detected as well. In particular, the regression-based models (GLMs and ANNs) with P2.LS and P2.S predictor configuration presented the best performance for this index, whereas the ones with local configuration (P2.L) presented the lowest skills.

Oppositely, the RAW outputs generally overestimated the amplitude of the annual cycle, excepting in the Patagonia region (R5) where most of the RAW outputs of the GCMs showed negative biases. In all regions, the RAW outputs exhibited a large dispersion among the different GCMs compared to the ESD simulations, depicted by larger boxes. Although this dispersion seems to be larger for the CMIP5 models (boxplots in green, Fig. 3c) than for those of CMIP6 (boxplots in purple, Fig. 3c), this comparison is not fair since the number of GCMs belonging to each experiment is imbalanced.

As a measure of the extreme warmest temperatures, the 98th percentile of the summer days distribution (DJF P98) was analysed for Tx. The observations exhibited the highest P98 in the northern regions of Argentina (R2, R3 and R4) where most of the stations presented P98 > 35ºC, while the lowest values were observed at the southern tip of the continent, in Patagonia region (R5) (Fig. 3a). The observed P98 were satisfactorily captured by the AN models, which highlighted from the rest of the ESD models with the smallest biases in all regions. The ANNs and GLMs families, instead, exhibited largest biases and tended to underestimate the warmest temperatures, especially the models that considered spatial predictors (S or LS configurations). Nevertheless, the biases from the ESD models were considerably smaller than the ones from the RAW outputs, which differed from the observations by up to 7.5ºC.

When analysing hot days (the number of days with Tx > 30ºC), the improvement of the ESD simulations compared to the RAW outputs was notable. Generally, the stations of northern Argentina (R2, R3 and R4), experienced Tx above 30ºC in about 90 to 150 days along the year (Fig. 3a). The statistically downscaled simulations showed skills to represent these values, differing in less than 15 days (considering absolute values) with the observations. Whereas RAW outputs presented a large dispersion among the GCMs performances in all regions and biases reaching almost 100 days in some of them. Commonly to both

approaches —ESD simulations and RAW outputs— the largest disagreement among GCM were detected in the northeast Argentina region (R2) which exhibited large boxes and highest biases. For this index —as for P98— differences were detected in the distributions of the CMIP5 and CMIP6 GCMs downscaled simulations. However, as mentioned above, these results are partly conditioned by the number of members in each experiment.

In the observed period the regional mean values of the median of the annual warm spell maxima (WarmAnnualMaxSpell) was close to 6 days in Pampas region and northeast Argentina (R1 and R2) and between 4 and 5 days in central-northwest Argentina and Patagonia region (R3 to R5) (Fig. 3a). In all regions, the downscaled simulations performed very similar and only the ANN.P2.S presented slightly small biases. The regression based models overestimated the duration of the warm spells while on the contrary, the AN models simulated shorter spells in all regions. The RAW outputs showed similar skills to the downscaled simulations to reproduce this index and this may be due to the percentile based threshold used for index construction which is independent from biases in the marginal distribution (Hertig et al., 2018)

Concerning Tn, the observed amplitude of the annual cycle (AnnualCycleAmp) was generally smaller than for Tx particularly in Patagonia Argentina (R5) (*Figura 4a*). The ESD simulations satisfactorily estimated this index and exhibited similar skills than for Tx. AN models typically underestimated the amplitude in all regions, while the performance of the ANN and GLM models varied depending on the region. The largest biases were identified in the Patagonia region (R5) and in northwest Argentina (R4) as a common feature of all ESD models. For the RAW simulations, the largest errors were exhibited in R4, where the amplitude of the annual cycle was underestimated by all the GCMs.

With focus on cold extremes, the winter 2nd percentile (P02) of Tn was assessed for the ESD and RAW simulations. During the reference period, observations presented P02 below zero in almost all regions, with minimum values in the stations over the Patagonia region (R5). Regarding the downscaled simulations, P02 was mostly overestimated by the ESD models in all regions. AN models well reproduce the observations and presented the smallest errors compared to the ANNs and GLMs which exhibited larger errors, especially in Argentina Patagonia (R5). In particular, GLMs showed a larger spread among the different GCMs simulations than the rest of the ESD models. RAW outputs presented high biases, with errors up to 7.5ºC for some GCMs, positive in all regions except in northwest Argentina (R4), in which positive and negative biases were exhibited and also a large disagreement among the GCMs.

The cold days (the number of days with Tn < 0ºC) were frequent in Patagonia and northwest Argentina (R4 and R5) during the period 1986–2005, with regional mean values of 75 and 45 days in the year, respectively (Fig. 4a). In northeast Argentina (R2), on the other hand, there were almost no cold days during the same period. The ESD simulations captured these regional features, specially the AN models that presented near zero errors in this index. GLMs and ANNs families presented higher errors than the AN models and commonly underestimated the number of cold days. In the case of the RAW simulations,

notable differences with the observations were identified in the regions R4 and R5, with biases of 50 days for some GCMs.

Regarding spells, the largest median of the annual cold spell maxima (ColdAnnualMaxSpell) was observed in the stations of norwest Argentina (R4) with a regional mean of 7 days and almost one day shorter in the regions of central and northeast Argentina (R1, R2 and R3). The length of the cold spells was generally underestimated by AN models while overestimated by the GLM models in all regions. The ANNs exhibited the more accurate values and presented biases between − 1 and 1 days among the different GCM, specially ANN.P2.L which exhibited the higher skills. Similar spell lengths were detected between RAW and the ESD simulations.

4.2 Climate change projections

In the previous section it was shown that ESD models were capable of reproducing the different characteristics of the observed maximum and minimum temperatures during the historical period when forced with different GCM, adding value to the RAW outputs. Here, another key aspect in the assessment of the ESD models was analysed and their ability to generate plausible future projections was assessed. The plausibility of the projections will be addressed taking into account the similarity with the projections provided by the RAW outputs (Manzanas et al. 2020; Baño-Medina et al. 2021) under the different scenarios and RCMs simulations available for the region, in order to provide a framework of comparison for future simulations.

a Far-future changes in mean climate

Increments in the mean values of the far future (2071–2100) from the RCP8.5 and SSP85 scenario with respect to the reference period (1986–2005) —delta changes— were evaluated for the ESD models, RAW and RCMs simulations. Figures 5 and 6 display these results for Tx and Tn for summer and winter austral seasons, respectively. For brevity only results for the ESD models with predictors P2.L, P2.S and P1.LS.a are shown for selected GCMs that will be more deeply analysed in the following section. The ESD models driven by the rest of the GCMs are available in the supplementary material (Figure S1 and Figure S2).

All simulations agreed on positive changes for Tx and Tn in the far future for all the regions of Argentina, and generally with a stronger signal of change in the warmest temperatures of the year (summer Tx). Nevertheless, some differences in the magnitude of these changes were detected among the different GCM and also within the ESD models, which were strongly influenced by the signal of the driving GCM and the statistical method considered. In addition, the climate sensitivity of each individual GCM was preserved in the ESD simulations (Figs. 5 and 6). The GCM which RAW outputs projected the highest levels of warming —e.g CanESM2 and CanESM5, Bukowski et al. (2020)— exhibited the largest delta changes in all ESD models. Whereas for GCMs with lower climate sensitivity —e.g NorESM1, Giorgi et al. (2012)— the ESD simulation presented a small increment of change. In the same way, the dynamical downscaling simulations (RCMs), showed the highest (lowest) values of delta changes in the Eta regional model driven by CanESM2 (RegCM and REMO driven by NorESM1).

Regarding Tx, the spatial distribution of the changes projected by the RAW simulations varied among the GCMs (Fig. 5). In general the stations from north Argentina (R1, R2, R3 and R4) exhibited the warmest signal (near 5–6 ºC). Moreover, for most of the GCMs the increases were larger in the stations along the north section of the subtropical Andes Mountain range (R4). On the other hand, in the Patagonia region, the increments of the summer Tx seemed to be smaller according to most of the RAW simulations. In addition, no remarkable differences were detected between the two emission scenarios (RCP8.5 and SSP585) which projected changes with similar magnitudes of warming.

When analysing the ESD simulations, the weakest signals of change were detected in the AN models with spatial predictors (P2.S, P1.LS.a) (*Figura 5*), with near zero values homogeneous across Argentina and almost identical in all GCMs. Bear in mind that the AN method is based on re-sampling observations and therefore, unprecedented warm temperatures —like the ones projected for the late future by the RCP8.5 and SPS85 scenarios— cannot be simulated by these models. In this sense, it was not surprising that AN models do not project large positive changes for the summer temperatures. Nevertheless, when considering local configuration (AN.P2.L), the AN models were closer to the RAW outputs, although still with low warming signal. In this regard, the spatial reduction by the EOFs in the S configuration (P2.S and P1.LS.a) may be adding some additional limitations to the AN method. Moreover, similar outcomes were identified between AN and ANN families clearly for P2.L and P2.S predictor configurations, typically underestimating the GCMs change signal. On the contrary, the GLM family presented the largest increases for the future, specially GLM.P2.S which tended to exacerbate the warming signal of the GCMs.

When comparing with the RAW outputs, the ESD models that only take into account local predictors (P2.L) showed similar spatial distributions and magnitude of the increases projected by the RAW simulations, regardless of the statistical technique considered. Furthermore, the RCM simulations also performed similarly to the ESD models with P2.L predictor configuration, although RegCM and REMO slightly underestimated the signal when comparing with their corresponding driving GCM RAW simulations. In this regard, the uncertainty found in future changes linked to the different statistical methods (ANs, GLMs and ANNs) was low —in terms of similarity between the different families and with the RCMs simulations—when considering the local configuration.

In comparison with Tx, the RAW outputs in general projected smaller increments (maximum 2–4 ºC) for the coldest temperatures (winter Tn) in the far future (Fig. 6). Overall, the GCMs exhibited the largest delta changes in the stations of northwest Argentina (R4) while these values decreased in magnitude toward the regions covering northeast Argentina (R1, R2 and R3). In the same line, the statistically downscaled simulations showed the strongest signals of change in the stations from northern Argentina. On the other hand, the RCM simulations presented a weaker signal of warming compared with the ESD simulations. Also, all RCM simulations projected very homogeneous increments across the country with no remarkable regional aspects.

Regarding the ESD simulations, the ANs, ANNs and GLMs performed very similarly, in contrast to the Tx results. In particular, compared to the Tx, a remarkable difference in the performance of AN.P2.S and

AN.P1.LS.a models were detected. As previously mentioned, the AN method is unable to simulate temperatures outside the range of the observations, being this restriction notable for summer temperatures. However, for winter temperatures –– since ANs were trained without any seasonal restrictions –– the range of observations are wider, covering synoptic situations that not only occur in winter but also in other seasons of the year. In this sense, future winter Tn may be more associated with situations prevailing in the warmer seasons of the year. Similar results were obtained for the winter Tx, although for brevity they were not shown. Nevertheless, the most distinctive differences detected within the ESD models were associated with the predictor configuration. The differences obtained by changes in the predictor sets (P1 or P2) were not as remarkable as the ones obtained by changes in the predictor configuration, also indicating that the future changes were not sensibly affected by the variation of predictors related to circulation variables which is the main difference between both predictors sets (Table 3). Generally the ESD models with only spatial configuration (P2.S) feature larger positive changes than the ones with local predictors (P2.L). For the spatial predictor configuration (S), information from the entire domain –reduced by the EOFs— is considered and the ESD models are generally more tightly related to large-scale processes (Huth 2004; Benestad et al. 2015). Whereas, with the local configuration (L), the ESD models only consider information from the neighbourhood and each station is exclusively influenced by the local changes. Therefore, more pronounced changes in the large-scale processes than in the local ones, could be amplifying the warming signal of the ESD models with S predictors. Similar to the summer Tx results, ESD models with local predictor configuration projected winter Tn changes rates in line with the RAW and RCMs simulations.

The increase in winter Tn and summer Tx in all regions of Argentina by the end of the century was systematic in all the simulations analysed, regardless of the source (ESD, RCMs or RAW) or statistical technique considered, indicating robustness in the future projections for the region. These increases were generally larger for the northern regions of Argentina, although the magnitude of these increases was variable among the different GCMs. In order to quantify the model uncertainty, the standard deviation (sd) of the delta changes projected by each ESD, RCMs and RAW model was computed, considering only the GCMs in common to CORDEX-CORE (Fig. 7). The highest values of sd (2-2.5º C) were detected in the RAW outputs, especially in the summer Tx associated with the different sensitivities of the GCMs already mentioned. Although these sensitivities are preserved across the different ESD models, the dispersion in the projections of the ESD models was considerably reduced, presenting sd values lower than RAW and comparable to the RCMs in both variables. For the warmest temperatures (summer Tx) wider dispersions were observed in northern and central Argentina in almost all ensembles (ESD, RAW and RCMs). While for the winter Tn, the sd values were lower and more homogeneous throughout Argentina. For both variables, the ESD models with L configuration exhibited closer values to the RCMs.

Based on the assessments of the ESD models in the historical and future scenarios, the ESD models with local configuration were selected to continue with the analysis of the future projections. In this regard, for each statistical method (ANs, ANNs, GLMs), one predictor configuration was preserved. Hereafter only results for GLM.P2.L, AN.P2.L and ANN.P2.L will be shown.

b. Regional time series

Lastly, future changes in the frequency of warm and cold extremes were explored. To this end, the time series of selected annual indices (Table 2) were analysed for the statistical and dynamical downscaling simulations and RAW outputs. The temporal evolution of the indices aggregated in regional mean values are displayed in Figs. 8 and 9 for CMIP5 and CMIP6 simulations separately. Again, for the CMIP5 ensemble, only the GCMs used to drive the RCMs (CanESM2, MPI-ESM-LR, MPI-ESM-MR and NorESM1) were considered. In this case, note that the ensemble of statistically downscaled simulations, being multi-method (12 simulations), is larger than the set of RCMs (5 simulations) and RAW (4 simulations) simulations. In the case of the CMIP6 models, the RAW ensemble presents 5 simulations while the ESD set is made up of 15 simulations.

Overall, all simulations projected an increase in the number of hot days for the end of the 21 century, larger for northeast Argentina (R2) —with 50–70 days above the reference period at the end of the century —. Similarly, a reduction in the number of cold days were detected in all simulations in norwest Argentina and the Patagonia region (R4 and R5).

Concerning hot days (Fig. 8*)*, the observations exhibited a marked increase from 2000 to 2018, in all the regions, which was detected by the ESD models ensemble for CMIP5 and CMIP6 simulations and also by the CMIP6 RAW ensemble mean. Whereas, for CMIP5, the RAW simulations tended to underestimate these changes and exhibited positive upward values a few years later. The RCM simulations stayed close to the RAW outputs in this period, and generally presented lower values with respect to the observations. For the mid and late future, the strongest signal of change was exhibited by the ESD simulations for both

scenarios RCP8.5 and SPS585. Depending on the region, the AN or GLM models ensemble projected the largest changes, although in regions R3, R4 and R5 all exhibited a similar rate of changes. In the case of CMIP5, the RAW and RCM simulations projected close values for the near and mid future, but they diverged at the end of the period. Furthermore, the dispersion among the different GCMs were in general similar for the RCM, RAW and ESD ensembles and estable during all the century. Regarding the CMIP6 simulation and SPS585 scenario, changes of the number of hot days were larger than the ones projected by the RAW CMIP5 simulations for the RCP8.5 scenario, especially in the regions R2 and R3. This was reflected in the ESD models as well, which exhibited highest values for CMIP6 simulations and also larger dispersion among the different ESD models.

For the number of cold days in R4 and R5 (Fig. 8), the dispersion among the RAW outputs considerably increased for CMIP5 and CMIP6 experiments, showing largest disagreement in the magnitude of the changes for the mid and late 21th century in northwest Argentina (R4). ESD models considerably reduced this dispersion, and also the RCM simulations in the case of CMIP5 simulations. A pronounced decrease of this index was detected in Patagonia region (R5) where generally, the RCM, RAW and ESD ensemble coincide in a reduction of about 20–40 days in a year for the late future. In this region, ESD and RAW ensemble simulations projected similar values while RCM slightly overestimated the negative trend.

Additionally, Fig. 9 shows the time series for the Tx90p index for all regions. All simulations agreed on warmer conditions for the future in all regions, projecting for the late 21th century an increase of more than 100 days in a year with Tx above the P90 percentile. In particular, similar outcomes were detected in the ESD models and RAW ensembles from CMIP5 in central and northeast Argentina (R1, R2 and R3) which coincided in a rapid increase of Tx90p, more accelerated than the projections of the RCM simulations. Whereas, in northwest Argentina (R4), ESD models performed similarly to the RCM ensemble and separated from the RAW simulations, projecting smaller values of future change. Among the regions, Patagonia (R5) exhibited the weaker signal for Tx90p, and a higher agreement among all simulations (Fig. 9). Changes depicted by the SSP585 from CMIP6 simulations were larger in all regions when compared to RCP85, for both ESD models and RAW outputs. Also a larger spread among the different GCMs was observed, more pronounced at the end of the century. In general, RAW outputs projected smaller (larger) changes than the ESD ensemble in R1 and R2 (R4 and R5) while performed similarly in central Argentina (R3).

Similar values were projected for Tn90p, although with a small spread among the simulations. For brevity, results from Tn90p are exhibited in the supplementary material (Figure S3 from supplementary material).

5. Discussion and conclusions

Argentina is a wide country with different climatic regions, where an increase in mean temperature and extremes is currently ongoing and affecting different socio-economic activities, putting pressure on local policy makers to design proper adaptation measures. Thus, delivering tailored climate information becomes essential to design and implement effective strategies in a climate change scenario. To this purpose, the use of Empirical Statistical Downscaling (ESD) strategies could help providing local climate information useful to address model uncertainty and ascertain our confidence in a global warming scenario.

In this study, a subset of ESD models taken from Balmaceda-Huarte and Bettolli (2022) were applied to a set of GCMs from the CMIP5 and CMIP6 experiments to statistically downscale maximum and minimum temperatures (Tx and Tn). This was done for the historical and future scenarios (RCP8.5 and SSP585) over the different climatic regions of Argentina. The selected ESD models were based on three different techniques: analogs (ANs), generalised linear models (GLMs) and artificial neural networks (ANNs); two predictor combinations (P1 and P2) with three different configurations (local, spatial or a combination of both).

A first assessment was carried out during the historical period, when statistically downscaled simulations were compared to the observations and the RAW model outputs. Results showed that ESD simulations added value to the RAW simulations, in mean values as well as in extreme indices, especially for Tx. All ESD simulations considerably reduced the seasonal biases (summer Tx and winter Tn) detected in the GCMs, similarly for the CMIP5 and CMIP6 ensembles. Furthermore, ESD models were able to represent multiple indices —which accounted for marginal and temporal aspects— based on Tx and Tn,

satisfactorily capturing the regional features of both variables. Statistical models exhibited higher skills in central and northeastern Argentina (R1 to R3), although depending on the aspect analysed, ESD models were more or less skillful based on the statistical technique (ANs, GLMs and ANNs) and predictor configuration considered. Notwithstanding, the performance of the ESD models during the historical period was similar to the validation period, when ESD models were forced with reanalysis data (Balmaceda-Huarte and Bettolli, 2022), evidencing the capability to be extrapolated to a different input space. The outcomes found in this work are in agreement with previous efforts within SSA, that demonstrated the added value of ESD compared to their driving GCMs in complex phenomena such as precipitation extremes (Olmo et al. 2022).

With the aim of evaluating the ability of the ESD models to generate plausible future projections, simulations from the worst-case scenarios (RCP8.5 and SSP585) obtained from the statistical and dynamical downscaling models (ESD and RCM), and RAW GCMs outputs were inter-compared in terms of their delta changes —far future (2071–2100) with respect to the reference period—. All simulations (RCMs, GCMs, ESD) agreed on positive changes in the most extreme temperatures throughout the year (summer Tx and winter Tn), strongest over northern Argentina and the northern section of the subtropical Andes. In this regard, ESD models showed potential to produce plausible climate projections. However, some differences in the magnitude of the future changes were detected among the GCMs and within ESD models, which preserved the climate sensitivity of their driving GCMs. For the statistical models, uncertainties in the magnitude of the future changes were associated to the technique considered —in the case of the summer Tx— and to the predictor configuration —in the case of the winter Tn— regardless of the driving GCM. Whereas, for both temperatures, no sensitivity was found related to the predictors set choice (P1 and P2). This uncertainty was larger for summer Tx, in which near zero delta changes were identified in the AN models that considered spatial predictors (P2.S, P1.LS.a), while large increases were projected for this variable by the GLM models, exacerbating the warming signal of the GCMs. In particular, this characteristic of the AN models —associated with its construction— was also documented by Gutierrez et al. (2013) and Casanueva et al. (2013) over the Iberian Peninsula. Differently to Tx, for winter Tn, the AN, ANN and GLM families performed very similarly and the most remarkable differences were connected with changes in the predictor configuration. In general, ESD models with only spatial configuration in the predictors (P2.S) featured larger changes than the ones with local predictors (P2.L). These differences may be related with changes in the large/local scale processes, which were more tightly related to the spatial/local predictor configuration and constrained the ESD models' projections differently. Particularly, the dimensionality reduction performed through the EOFs could be also affecting the future change rates. This discussion was partly addressed by Huth (2002), who found that the number of principal components (PCs) retained in the regression models has a considerable effect on temperature future projections over central and western Europe. In addition, Sachindra et al. (2013) and Panda et al. (2022) showed that using PCs as input data can affect the performance of the ESD models in climate change applications, related to the different data space (reanalysis/GCMs) in which ESD models are trained and applied. To circumvent this, Benestad (2001) proposes using combined PCs

between the predictors of the reanalysis and the GCMs, to minimise the errors associated with the downscaling of future climate scenarios.

The RCM simulations stayed close to the rate of changes projected by the ESD models —specially the ones with L predictor configuration— for the summer Tx, while generally exhibited a weaker signal of warming for the winter Tn compared with the ESD and RAW outputs. Notwithstanding, for both variables, the dispersion within each set of simulations (RCMs and ESD models) was similar, and both smaller in relation to the RAW CMIP5 ensemble. Furthermore, the mean changes detected here are in agreement with previous works, which identified a future warming amplification over the subtropical Andes and northern Argentina when using CMIP5 and CMIP6 RAW simulations and RCMs for mean surface temperature (Blazquez and Solman 2023; Bustos Usta et al., 2022; Gulizia et al. 2022; Coppola et al. 2021; Almazroui et al. 2021; Pabón-Caicedo et al., 2020; Zazulie et al., 2018); for extreme temperature indices (LagosZúñiga et al. 2022; Reboita et al. 2022) and compound temperature-rainfall events (Olmo et al. 2022a; Collazo et al. 2023). In line with this, the evaluation of the regional future changes in the frequency of warm and cold extremes also depicted a robust signal of warming for Argentina. All simulations agreed on an increase (decrease) in the number of hot (cold) days by the end of the 21st century, more accelerated for the region of northeast Argentina (norwest Argentina and Patagonia). Regarding hot days, the strongest signal of change was exhibited by the ESD simulations, while the RCM simulations exhibited the weakest signal of change. For this index, the dispersion among the different GCMs was similar for the RCM, RAW and ESD simulations. For the number of cold days, instead, the dispersion among the RAW outputs considerably increased for CMIP5 and CMIP6 experiments, showing the largest disagreement in the change rates for the mid- and late-21st century, especially in northwest Argentina (R4). ESD models considerably reduced this dispersion, and also the RCM simulations for the CMIP5 simulations. A pronounced decrease of the number of cold days was detected in the Patagonia region (R5), in line with the results of Gulizia et al. (2022) for the index frost day using CMIP5 RAW simulations. In particular, this reduction could represent a significant impact for the region in terms of snow availability and the conservation of glaciers (Zazulie et al. 2018). In the same line, for the percentile-based indices (Tx90p and Tn90p) all simulations agreed on warmer conditions, although with larger spread among simulations in Tx90p. Results of these indices were in agreement with Rusticucci and Zazulie (2021) that analysed RAW simulations from a set of CMIP5 models, although the authors found a faster rate of warming in Tn90p than Tx90p not clearly identified here. Using RCM simulations, Reboita et al. (2022) and López-Franca et al. (2016) also found a more pronounced warming in Tn90p, but limited to the region north of 20° in SSA and La Plata basin. Note, however, that in these studies the indices were calculated on a seasonal basis (summer and winter), whereas in the present work they were computed annually. In this regard, the differences in the intensity of the changes found could be partly attributed to a compensation between Tx and Tn during the transition seasons.

Overall, this is a novel study that provides insight into the suitability of different ESD models —based on multiple statistical methods, predictors variables and configurations— for the simulation of historical local climate and the methodological sensitivity to generate reliable climate projections. The importance of using the different simulations available for Southern South America to comprehensively analyse

regional climate change signals and their uncertainty became evident in this work, where depending on the temperature aspect studied different levels of agreement were found. In this sense, our projections built on multi-model and multi-method ensembles are key to handle the uncertainty in the future climate over different regions of Argentina, where high resolution simulations are still scarce. However, some limitations of the ESD simulations need to be further explored, like the stationary assumption (Vrac et al. 2007) and the use of other state-of-the-art statistical methods (Quesada-Chacón et al. 2021; Legasa et al. 2023). Furthermore, employing hybrid approaches combining dynamical and statistical downscaling such as pseudo-reality experiments and emulators (Hernanz et al. 2022b; Doury et al. 2023; Boe et al. 2023) will be explored in follow-up studies to tackle these challenges over the region.

Declarations

Ethics approval and consent to participate

Not applicable.

Consent for publication

Not applicable.

Competing interests

The authors have no relevant financial or non-financial interests to disclose.

Authors' contributions

All authors contributed to the study conception and design. Material preparation, data collection and analysis were performed by Rocio Balmaceda-Huarte. The original draft was written by Rocio Balmaceda-Huarte and Matias Olmo, and all authors made substantial contributions. Supervision was performed by María Laura Bettolli. All authors read and approved the final manuscript.

Availability of data and materials

The gridded datasets used in this study are available online. ERA-Interim reanalysis (ERA, Dee et al. 2011) https://www.ecmwf.int/en/forecasts/datasets/reanalysis-datasets/era-interim. Simulations from CMIP5 and CMIP6 modelling experiment (Taylor et al. 2012; Eyring et al. 2016) https://esgf-node.llnl.gov.

Funding

This work was supported by the University of Buenos Aires 20020220200111BA and the ANPCyT PICT-2018-02496 and PICT 2019-02933 projects.

References

1. Almazroui, M., Ashfaq, M., Islam, M.N. et al. (2021) Assessment of CMIP6 Performance and Projected Temperature and Precipitation Changes Over South America. Earth Syst Environ 5, 155–183 . https://doi.org/10.1007/s41748-021-00233-6
2. Alexander, L. V., & Arblaster, J. M. (2017) Historical and projected trends in temperature and precipitation extremes in Australia in observations and CMIP5. Weather and climate extremes, 15, 34-56.
3. Araya-Osses, D., Casanueva, A., Román-Figueroa, C., Uribe, J. M., y Paneque, M. (2020) Climate change projections of temperature and precipitation in chile based on statistical downscaling. Climate Dynamics, 54, 4309–4330.
4. Asong, Z. E., Khaliq, M., y Wheater, H., (2016) Multisite multivariate modeling of daily precipitation and temperature in the Canadian prairie provinces using generalized linear models. Climate Dynamics, 47, 2901–2921.
5. Avila-Diaz, A., Torres, R.R., Zuluaga, C.F. et al. (2023) Current and Future Climate Extremes Over Latin America and Caribbean: Assessing Earth System Models from High Resolution Model Intercomparison Project (HighResMIP). Earth Syst Environ 7, 99–130 . https://doi.org/10.1007/s41748-022-00337-7
6. Baño-Medina, J., Manzanas, R., Cimadevilla, E., Fernández, J., González-Abad, J., Cofiño,
7. A. S., y Gutiérrez, J. M. (2022). Downscaling multi-model climate projection ensembles with deep learning (deepesd): contribution to cordex eur-44. Geoscientific Model Development, 15 (17), 6747–6758.
8. Baño-Medina, J., Manzanas, R., y Gutiérrez, J. M. (2021) On the suitability of deep convolutional neural networks for continental-wide downscaling of climate change projections. Climate Dynamics, 57, 2941–2951.
9. Barros, V. R., Grimm, A. M., y Doyle, M. E. (2002) Relationship between temperature and circulation in southeastern south america and its influence from el ninño and la niña events. Journal of the Meteorological Society of Japan. Ser. II, 80 (1), 21–32.
10. Beck, H. E., Zimmermann, N. E., McVicar, T. R., Vergopolan, N., Berg, A., y Wood, E. F., (2018) Present and future köppen-geiger climate classification maps at 1-km resolution. Scientific data, 5 (1), 1–12.
11. Bedia, J., Baño-Medina, J., Legasa, M. N., Iturbide, M., Manzanas, R., Herrera, S., ... & Gutiérrez, J. M. (2020) Statistical downscaling with the downscaleR package (v3. 1.0): contribution to the VALUE intercomparison experiment. Geoscientific Model Development, 13(3), 1711-1735.
12. Benestad, R. E. (2001) A comparison between two empirical downscaling strategies. International Journal of Climatology: A Journal of the Royal Meteorological Society, 21 (13), 1645–1668.
13. Bettolli, M. L., y Penalba, O. C. (2018) Statistical downscaling of daily precipitation and temperatures in southern la plata basin. International Journal of Climatology, 38 (9), 3705–3722.
14. Blázquez, J., y Solman, S. A. (2023) Temperature and precipitation biases in cordex rcm simulations over south america: possible origin and impacts on the regional climate change signal. Climate Dynamics, 1–14.

15. Boé, J., Mass, A. & Deman, J.(2023) A simple hybrid statistical–dynamical downscaling method for emulating regional climate models over Western Europe. Evaluation, application, and role of added value?. Clim Dyn 61, 271–294 . https://doi.org/10.1007/s00382-022-06552-2
16. Bustos Usta, D. F., Teymouri, M., y Chatterjee, U. (2021) Projections of temperature changes over south america during the twenty-first century using cmip6 models. GeoJournal, 1–25.
17. Carril AF, Cavalcanti IFA, Menéndez CG, Sörensson A and others (2016) Extreme events in the La Plata basin: a retrospective analysis of what we have learned during CLARIS-LPB project. Clim Res 68:95-116. https://doi.org/10.3354/cr01374
18. Casanueva, A., Herrera, S., Fernández, J., Frías, M., y Gutiérrez, J. M. (2013) Evaluation and projection of daily temperature percentiles from statistical and dynamical downscaling methods. Natural Hazards and Earth System Sciences, 13 (8), 2089–2099.
19. Chou, S. C., Lyra, A., Mourão, C., Dereczynski, C., Pilotto, I., Gomes, J., ... & Chagas, D. (2014) Evaluation of the Eta simulations nested in three global climate models. American Journal of Climate Change, 3(05), 438.
20. Collazo, S., Barrucand, M. & Rusticucci, M. (2022) Evaluation of CMIP6 models in the representation of observed extreme temperature indices trends in South America. Climatic Change 172, 21 https://doi.org/10.1007/s10584-022-03376-1
21. Collazo, S., Barrucand, M. & Rusticucci, M. (2023) Hot and dry compound events in South America: present climate and future projections, and their association with the Pacific Ocean. Nat Hazards 119, 299–323 . https://doi.org/10.1007/s11069-023-06119-2
22. Coppola, E., Raffaele, F., Giorgi, F. et al. (2021) Climate hazard indices projections based on CORDEX-CORE, CMIP5 and CMIP6 ensemble. Clim Dyn 57, 1293–1383 . https://doi.org/10.1007/s00382-021-05640-z
23. Coronato, T. and Zaninelli, P. G. and Abalone, R. and Carril, A. F. (2023) Climate Change Impact Studies on the Cooling Energy Demand of Social Housing in Central-Eastern Argentina. Available at SSRN: http://dx.doi.org/10.2139/ssrn.4390513.
24. De Luca, P., & Donat, M. G. (2023). Projected changes in hot, dry, and compound hot-dry extremes over global land regions. Geophysical Research Letters, 50, e2022GL102493. https://doi.org/10.1029/2022GL102493
25. Dee, D. P., Uppala, S. M., Simmons, A. J., Berrisford, P., Poli, P., Kobayashi, S., ... & Vitart, F. (2011). The ERA-Interim reanalysis: Configuration and performance of the data assimilation system. Quarterly Journal of the royal meteorological society, 137(656), 553-597.
26. Doury, A., Somot, S., Gadat, S. et al. (2023) Regional climate model emulator based on deep learning: concept and first evaluation of a novel hybrid downscaling approach. Clim Dyn 60, 1751–1779. https://doi.org/10.1007/s00382-022-06343-9.
27. Engdaw, M. M., Steiner, A. K., Hegerl, G. C., & Ballinger, A. P. (2023). Attribution of observed changes in extreme temperatures to anthropogenic forcing using CMIP6 models. Weather and Climate Extremes, 39, 100548.

28. Eyring, V., Bony, S., Meehl, G. A., Senior, C. A., Stevens, B., Stouffer, R. J., y Taylor, K. E. (2016). Overview of the coupled model intercomparison project phase 6 (cmip6) experimental design and organization. Geoscientific Model Development, 9 (5), 1937–1958.
29. Fan, L. J., Yan, Z. W., Chen, D., & Li, Z. (2022). Assessment of Central Asian heat extremes by statistical downscaling: Validation and future projection for 2015–2100. Advances in Climate Change Research, 13(1), 14-27.
30. Fontan S and Rusticucci M (2021) Climate and Health in Buenos Aires: A Review on Climate Impact on Human Health Studies Between 1995 and 2015. Front. Environ. Sci. 8:528408. doi: 10.3389/fenvs.2020.528408
31. Giorgetta, M. A., Jungclaus, J., Reick, C. H., Legutke, S., Bader, J., Böttinger, M., ... & Stevens, B. (2013) Climate and carbon cycle changes from 1850 to 2100 in MPI-ESM simulations for the Coupled Model Intercomparison Project phase 5. Journal of Advances in Modeling Earth Systems, 5(3), 572-597.
32. Giorgi, F. (2019). Thirty years of regional climate modeling: where are we and where are we going next? Journal of Geophysical Research: Atmospheres, 124 (11), 5696–5723.
33. Giorgi, F., Jones, C., & Asrar, G. R. (2009) Addressing climate information needs at the regional level: the CORDEX framework. World Meteorological Organization (WMO) Bulletin, 58(3), 175.
34. Giorgi, F., Coppola, E., Solmon, F., Mariotti, L., Sylla, M. B., Bi, X., ... & Brankovic, C. (2012) RegCM4: model description and preliminary tests over multiple CORDEX domains. Climate Research, 52, 7-29.
35. Gutiérrez, J. M., San-Martín, D., Brands, S., Manzanas, R., y Herrera, S. (2013) Reassessing statistical downscaling techniques for their robust application under climate change conditions. Journal of Climate, 26 (1), 171–188.
36. Gutowski Jr, W. J., Giorgi, F., Timbal, B., Frigon, A., Jacob, D., Kang, H. S., ... & Tangang, F. (2016) WCRP coordinated regional downscaling experiment (CORDEX): a diagnostic MIP for CMIP6.
37. Hazeleger, W., y coautores (2010) Ec-earth: a seamless earth-system prediction approach in action. Bulletin of the American Meteorological Society, 91 (10), 1357–1364.
38. Hernanz, A., García-Valero, J. A., Domínguez, M., Ramos-Calzado, P., Pastor-Saavedra, M. A., y Rodríguez-Camino, E. (2022a). Evaluation of statistical downscaling methods for climate change projections over spain: present conditions with perfect predictors. International Journal of Climatology, 42 (2), 762–776.
39. Hernanz, A., García-Valero, J. A., Domínguez, M., & Rodríguez-Camino, E. (2022b). Evaluation of statistical downscaling methods for climate change projections over Spain: Future conditions with pseudo reality (transferability experiment). International Journal of Climatology, 42(7), 3987–4000. https://doi.org/10.1002/joc.7464
40. Hurrell, J. W., y coautores, 2013. The community earth system model: a framework for collaborative research. Bulletin of the American Meteorological Society, 94 (9), 1339–1360.
41. Huth, R. (2002). Statistical downscaling of daily temperature in central europe. Journal of Climate, 15 (13), 1731–1742.

42. Huth, R., Mikšovskỳ, J., Štěpánek, P., Belda, M., Farda, A., Chládová, Z., y Pišoft, P. (2015) Comparative validation of statistical and dynamical downscaling models on a dense grid in central europe: temperature. Theoretical and Applied Climatology, 120, 533–553
43. Huth, R. (2004) Sensitivity of local daily temperature change estimates to the selection of downscaling models and predictors. Journal of Climate, 17 (3), 640–652.
44. Huth, R. (1999) Statistical downscaling in central europe: evaluation of methods and potential predictors. Climate Research, 13 (2), 91–101.
45. Iturbide, M., Bedia, J., Herrera, S., Baño-Medina, J., Fernández, J., Frías, M. D., ... & Gutiérrez, J. M. (2019) The R-based climate4R open framework for reproducible climate data access and post-processing. Environmental Modelling & Software, 111, 42-54.
46. Jacob, D., Elizalde, A., Haensler, A., Hagemann, S., Kumar, P., Podzun, R., ... & Wilhelm, C. (2012) Assessing the transferability of the regional climate model REMO to different coordinated regional climate downscaling experiment (CORDEX) regions. Atmosphere, 3(1), 181-199.
47. Kirchmeier-Young, M. C., Zwiers, F. W., Gillett, N. P., y Cannon, A. J. (2017) Attributing extreme fire risk in western canada to human emissions. Climatic Change, 144, 365–379.
48. Lagos-Zúñiga, M., Balmaceda-Huarte, R., Regoto, P., Torrez, L., Olmo, M., Lyra, A., Pareja-
49. Quispe, D., y Bettolli, M. L. (2022) Extreme indices of temperature and precipitation in south america: trends and intercomparison of regional climate models. Climate Dynamics, 1–22.
50. Legasa, M. N., Thao, S., Vrac, M., & Manzanas, R. (2023) Assessing three perfect prognosis methods for statistical downscaling of climate change precipitation scenarios. Geophysical Research Letters, 50, e2022GL102525. https://doi.org/10.1029/2022GL102525
51. López-Franca, N., Zaninelli, P. G., Carril, A. F., Menéndez, C. G., y Sánchez, E., 2016. Changes in temperature extremes for 21st century scenarios over south america derived from a multi-model ensemble of regional climate models. Climate Research, 68 (2-3), 151–167.
52. Manzanas, R., Fiwa, L., Vanya, C., Kanamaru, H., y Gutiérrez, J. M. (2020) Statistical downscaling or bias adjustment? a case study involving implausible climate change projections of precipitation in malawi. Climatic Change, 162, 1437–1453.
53. Maraun, D., y Widmann, M. (2018) Statistical downscaling and bias correction for climate research. Cambridge University Press.
54. Maraun, D., y coautores, (2015) Value: A framework to validate downscaling approaches for climate change studies. Earth's Future, 3 (1), 1–14.
55. Miranda, V.F.V.V., dos Santos, D.M., Peres, L.F. et al. (2023) Heat stress in South America over the last four decades: a bioclimatic analysis. Theor Appl Climatol . https://doi.org/10.1007/s00704-023-04668-x
56. Müller, W. A., Jungclaus, J. H., Mauritsen, T., Baehr, J., Bittner, M., Budich, R., ... & Marotzke, J. (2018) A higher-resolution version of the max planck institute earth system model (MPI-ESM1. 2-HR). Journal of Advances in Modeling Earth Systems, 10(7), 1383-1413.

57. Olmo, M., Balmaceda-Huarte, R., y Bettolli, M. L. (2022a) Multi-model ensemble of statistically downscaled gcms over southeastern south america: historical evaluation and future projections of daily precipitation with focus on extremes. Climate Dynamics, 59 (9-10), 3051–3068.
58. Olmo, M. E., Weber, T., Teichmann, C., & Bettolli, M. L. (2022b) Compound Events in South America Using the CORDEX-CORE Ensemble: Current Climate Conditions and Future Projections in a Global Warming Scenario. Journal of Geophysical Research: Atmospheres, 127(21), e2022JD037708.
59. Pabón-Caicedo, J. D., Arias, P. A., Carril, A. F., Espinoza, J. C., Borrel, L. F., Goubanova, K., and Villalba, R. (2020) Observed and projected hydroclimate changes in the Andes. Frontiers in Earth Science, 8, 61.
60. Panda, K. C., Singh, R., Thakural, L., y Sahoo, D. P. (2022) Representative grid location multivariate adaptive regression spline (rgl-mars) algorithm for downscaling dry and wet season rainfall. Journal of hydrology, 605, 127 381.
61. Reboita, M. S., Kuki, C. A. C., Marrafon, V. H., de Souza, C. A., Ferreira, G. W. S., Teodoro,
62. T., y Lima, J. W. M. (2022) South america climate change revealed through climate indices projected by gcms and eta-rcm ensembles. Climate Dynamics, 58 (1-2), 459–485.
63. Rumelhart, D. E., Hinton, G. E., y Williams, R. J. (1986) Learning representations by backpropagating errors. nature, 323 (6088), 533–536.
64. Rusticucci, M., y Zazulie, N., (2021) Attribution and projections of temperature extreme trends in south america based on cmip5 models. Annals of the New York Academy of Sciences, 1504 (1), 154–166.
65. Sachindra, D., Huang, F., Barton, A., y Perera, B. (2013) Least square support vector and multilinear regression for statistically downscaling general circulation model outputs to catchment streamflows. International Journal of Climatology, 33 (5), 1087–1106.
66. Scoccimarro, E., Gualdi, S., Bellucci, A., Sanna, A., Giuseppe Fogli, P., Manzini, E., ... & Navarra, A. (2011) Effects of tropical cyclones on ocean heat transport in a high-resolution coupled general circulation model. Journal of Climate, 24(16), 4368-4384.
67. Suli, S., Barriopedro, D., García–Herrera, R., & Rusticucci, M. (2023) Regionalisation of heat waves in southern South America. Weather and Climate Extremes, 40, 100569.
68. Swart, N. C., Cole, J. N., Kharin, V. V., Lazare, M., Scinocca, J. F., Gillett, N. P., ... & Winter, B. (2019) The Canadian earth system model version 5 (CanESM5. 0.3). Geoscientific Model Development, 12(11), 4823-4873.
69. Taylor, K. E., Stouffer, R. J., y Meehl, G. A., (2012) An overview of cmip5 and the experiment design. Bulletin of the American meteorological Society, 93 (4), 485–498.
70. Volodin, E., Dianskii, N., y Gusev, A., (2010) Simulating present-day climate with the inmcm4.0 coupled model of the atmospheric and oceanic general circulations. Izvestiya, Atmospheric and Oceanic Physics, 46, 414–431.
71. Volodin, E. M., Mortikov, E. V., Kostrykin, S. V., Galin, V. Y., Lykossov, V. N., Gritsun, A. S., ... & Iakovlev, N. G. (2017) Simulation of the present-day climate with the climate model INMCM5. Climate

dynamics, 49, 3715-3734.

72. Vrac, M., y Ayar, P. V. (2017) Influence of bias correcting predictors on statistical downscaling models. Journal of Applied Meteorology and Climatology, 56 (1), 5–26.
73. Weare, B. C., Cagnazzo, C., Fogli, P. G., Manzini, E., y Navarra, A. (2012) Madden-julian oscillation in a climate model with a well-resolved stratosphere. Journal of Geophysical Research: Atmospheres, 117 (D1).
74. Zazulie, N., Rusticucci, M., y Raga, G. B. (2017) Regional climate of the subtropical central andes using high-resolution cmip5 models—part i: past performance (1980–2005). Climate dynamics, 49, 3937–3957.
75. Zazulie, N., Rusticucci, M., y Raga, G. B. (2018) Regional climate of the subtropical central andes using high-resolution cmip5 models. part ii: future projections for the twenty-first century. Climate dynamics, 51, 2913–2925.
76. Zorita, E., y Von Storch, H. (1999) The analog method as a simple statistical downscaling technique: Comparison with more complicated methods. Journal of climate, 12 (8), 2474–2489.

Figures

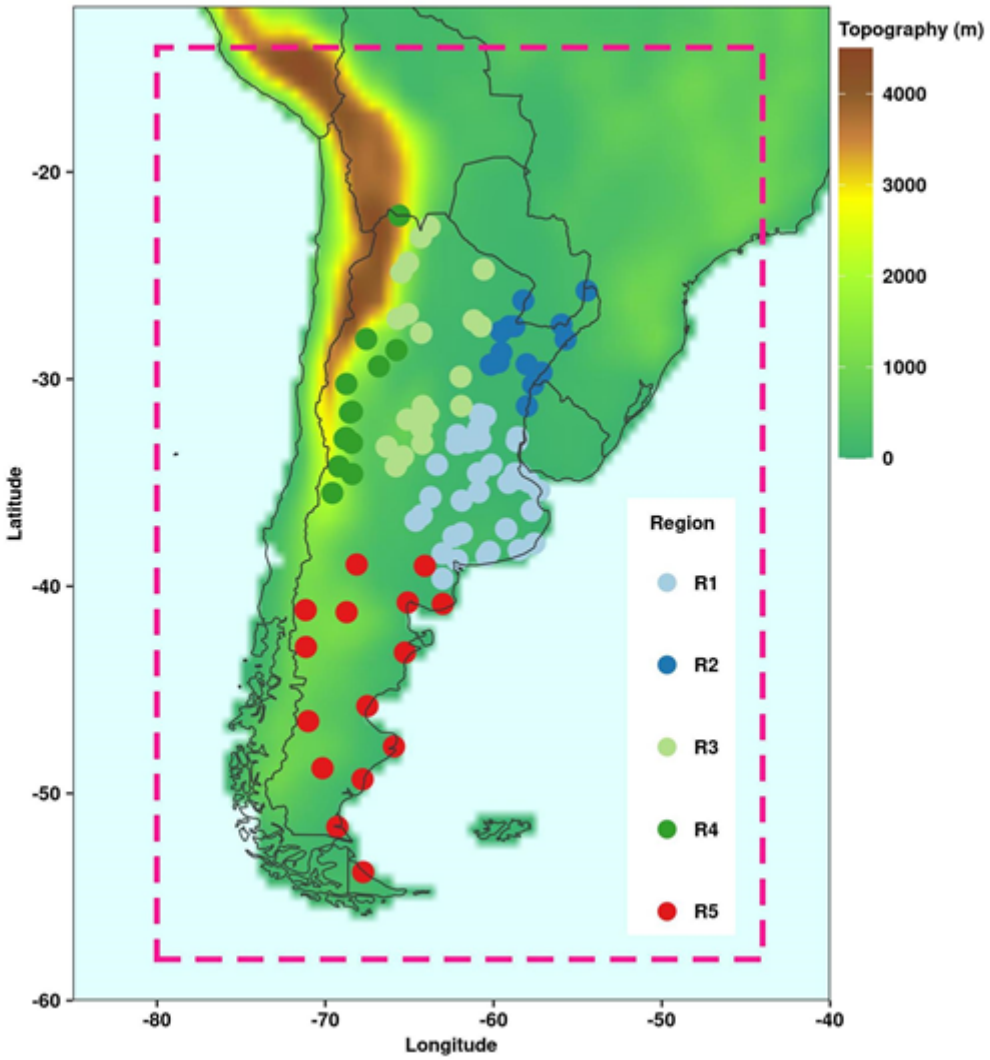

Figure 1

Meteorological stations used in this study, coloured by region (numbered from R1 to R5). The pink box represents the domain considered for the predictor sets of the ESD models. Shaded colours indicate the SSA elevation (taken from the ERA-Interim reanalysis) expressed in metres.

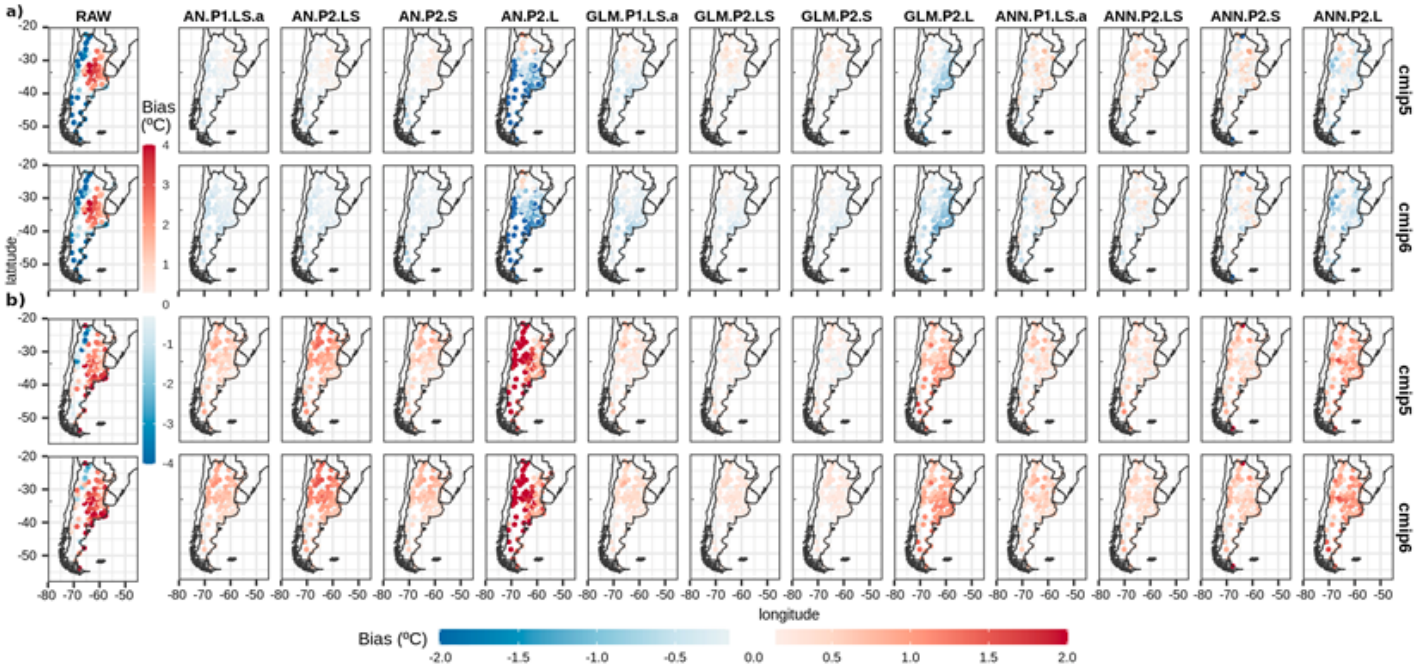

Figure 2

Differences in the mean values (bias) of the historical period (1979–2005) between the ensemble mean of CMIP5 and CMIP6 GCMs and the observations (reference) considering : (column 1) raw data (RAW); (column 2-8) the different ESD models. Results are displayed for Tx (a) and Tn (b) for summer (DFJ) and winter (JJA) season, respectively. For CMIP5 (CMIP6) the historical period is 1979-2005 (1979-2014).

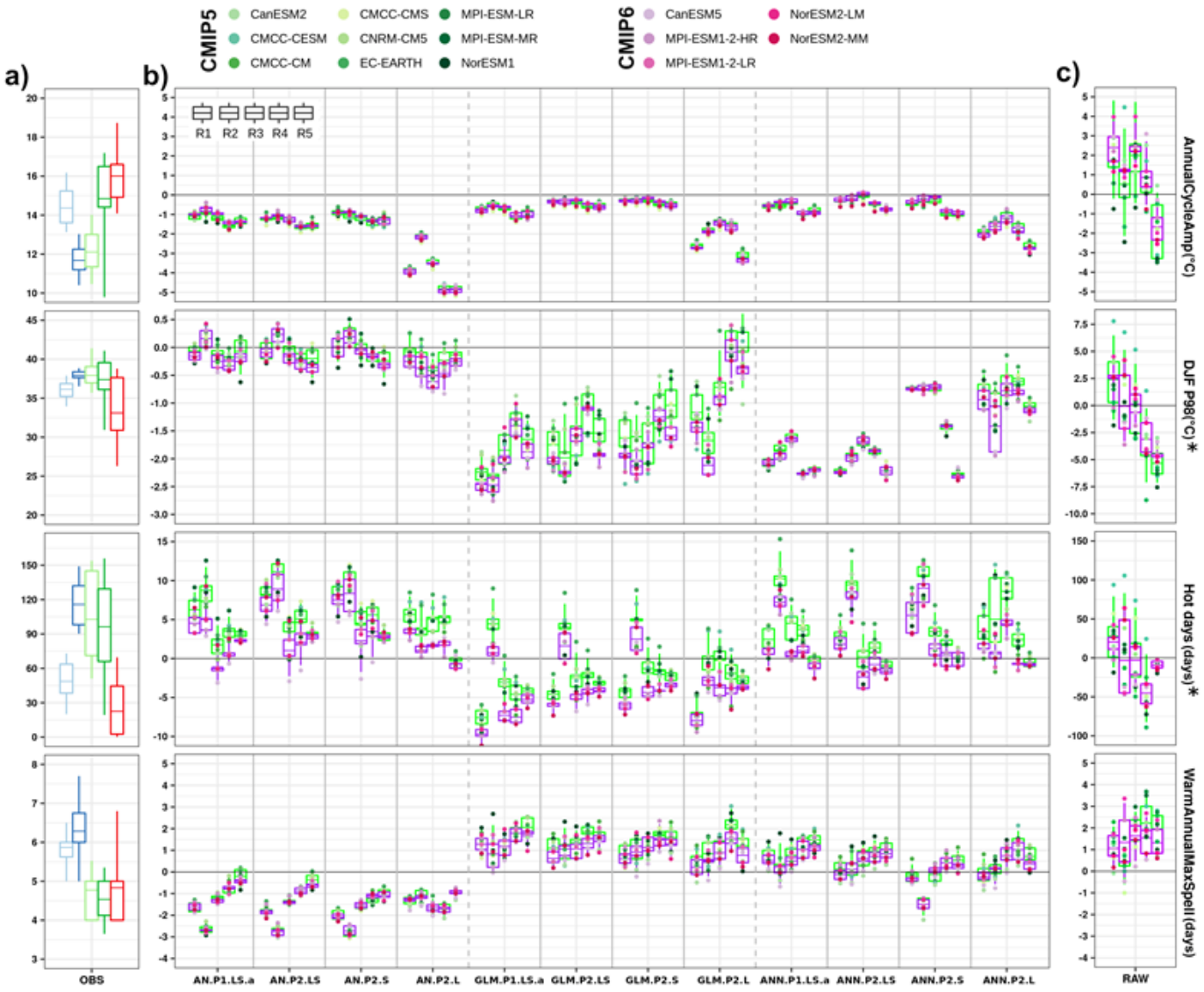

Figure 3

Boxplot diagrams that shows a) the spatial distribution of the indices from Table 4 calculated with the observed values for Tx in each region, ordered from left to right (R1-R5) following the colours from Figure 1. b) indices regional mean values estimates for each ESD model; and c) RAW simulation for each GCMs. In b) and c), the results are expressed in terms of bias, and the regions are shown ordered from left to right (R1-R5). In green (violet) boxplots, the results for CMIP5 (CMIP6) models are displayed, and different shades of green (violet) indicate each individual GCM. In each boxplot diagram, the center mark corresponds to the mean, and the lower and upper edges represent the 25th and 75th percentiles. The whiskers extend to the 5th and 95th percentiles. Indices with different scales among ESD and RAW simulations are denoted with an asterisk.

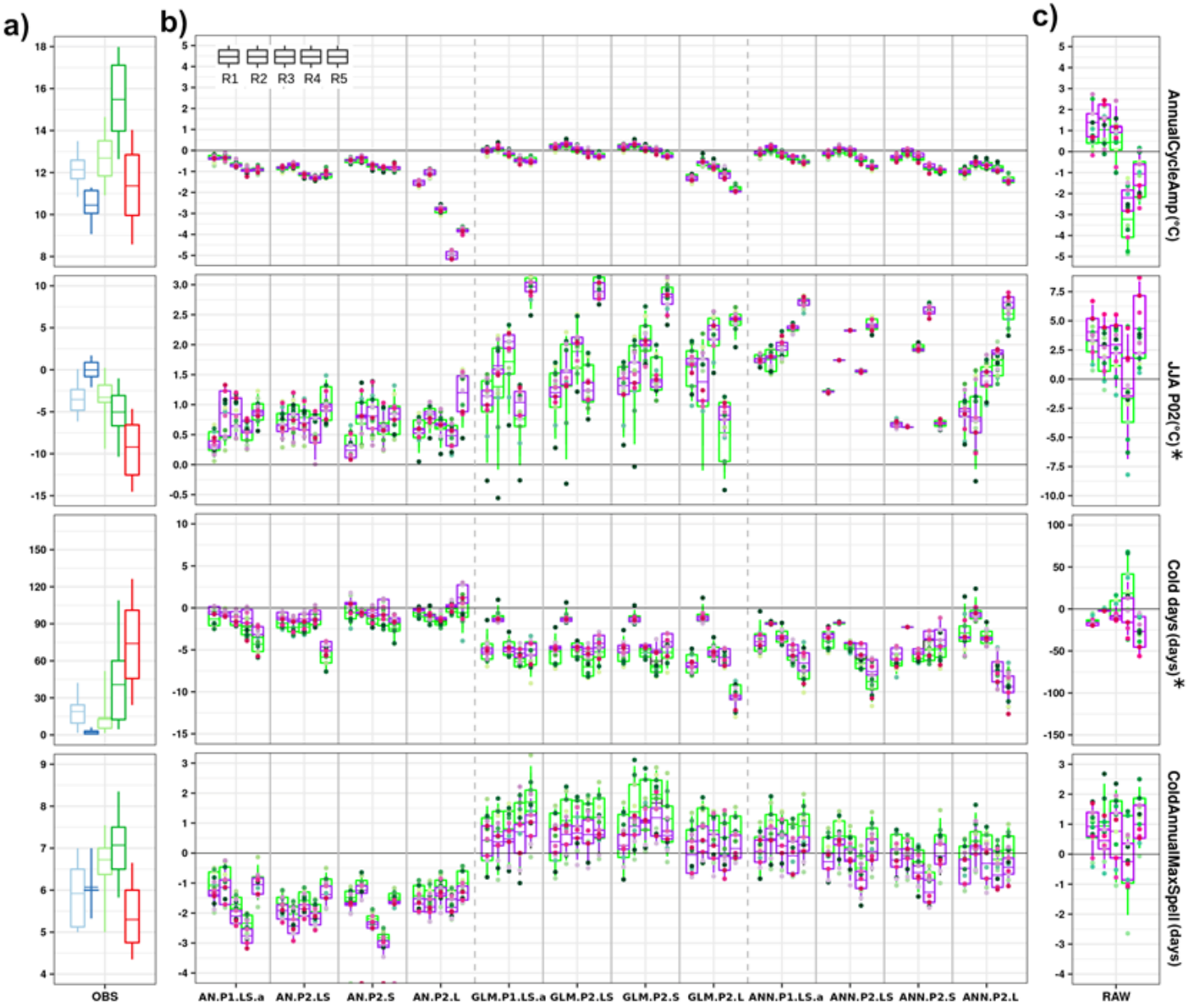

Figure 4

Similar to Figure 3 for indices from Table 4 for Tn.

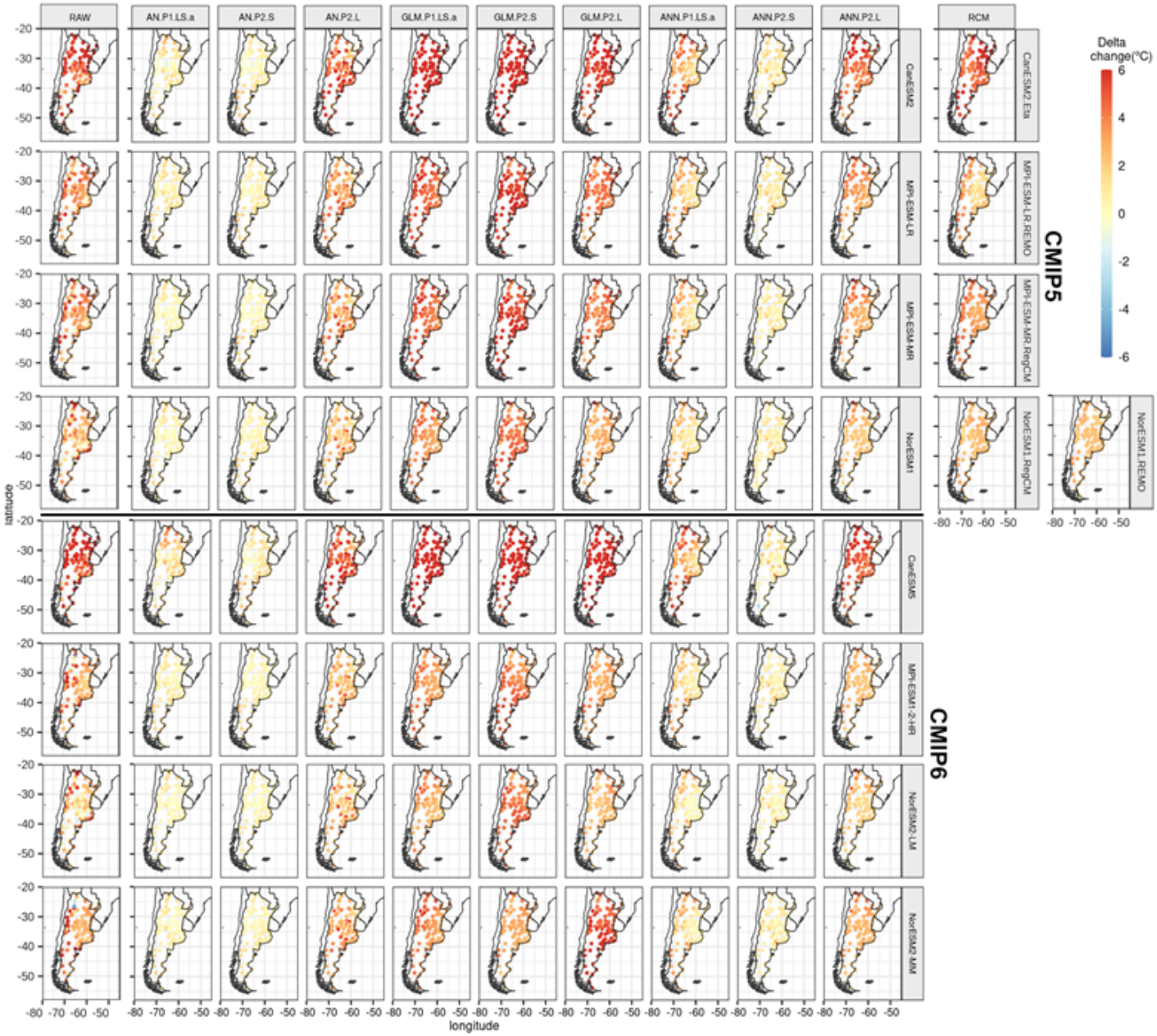

Figure 5

Changes projected for Tx in the far future (2071-2100) w.r.t the reference period (1986-2005) during summer (DJF) considering: the raw outputs of the GCMs (RAW) and simulations from ESD and RCMs (for available GCMs) for each individual GCM, taking the worst-case scenarios RCP8.5 and SP585.

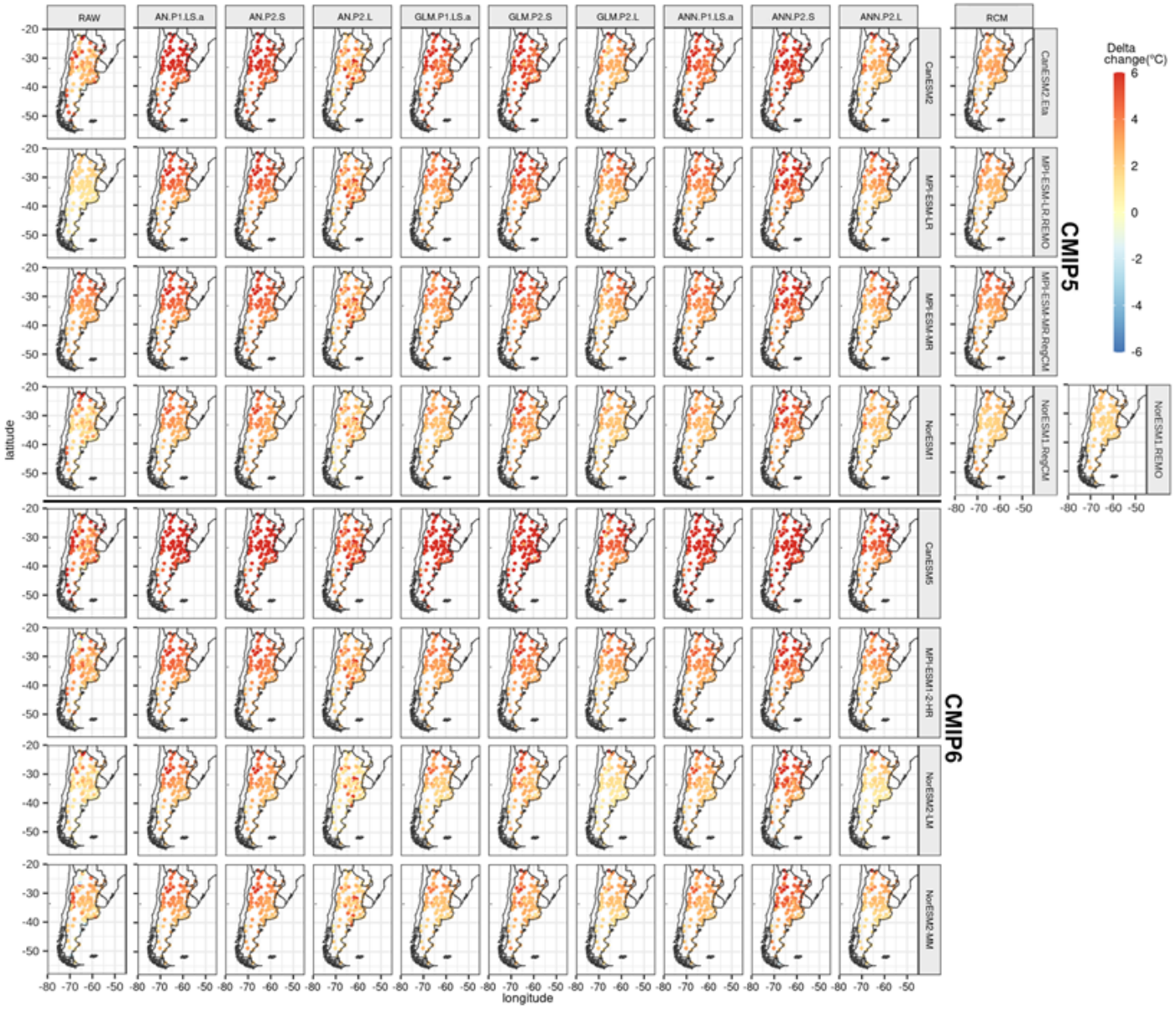

Figure 6

Similar to Figure 5 for Tn during the winter season (JJA).

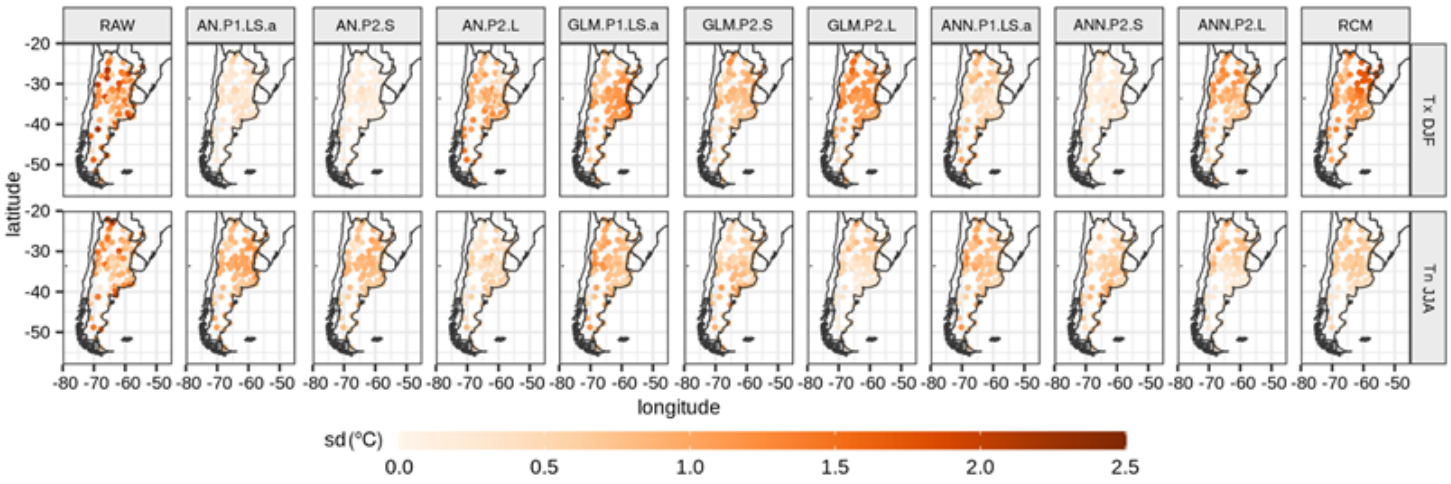

Figure 7

Uncertainty of the projected values from Figures 5 and 6 measured in terms of standard deviation (sd) calculated for each set of RAW, ESD models, and RCMs simulations for summer Tx (Tx DJF) and winter Tn (Tn JJA). To compute the standard deviation, only the GCMs forcing CORDEX-CORE RCMs (Table 4) were considered.

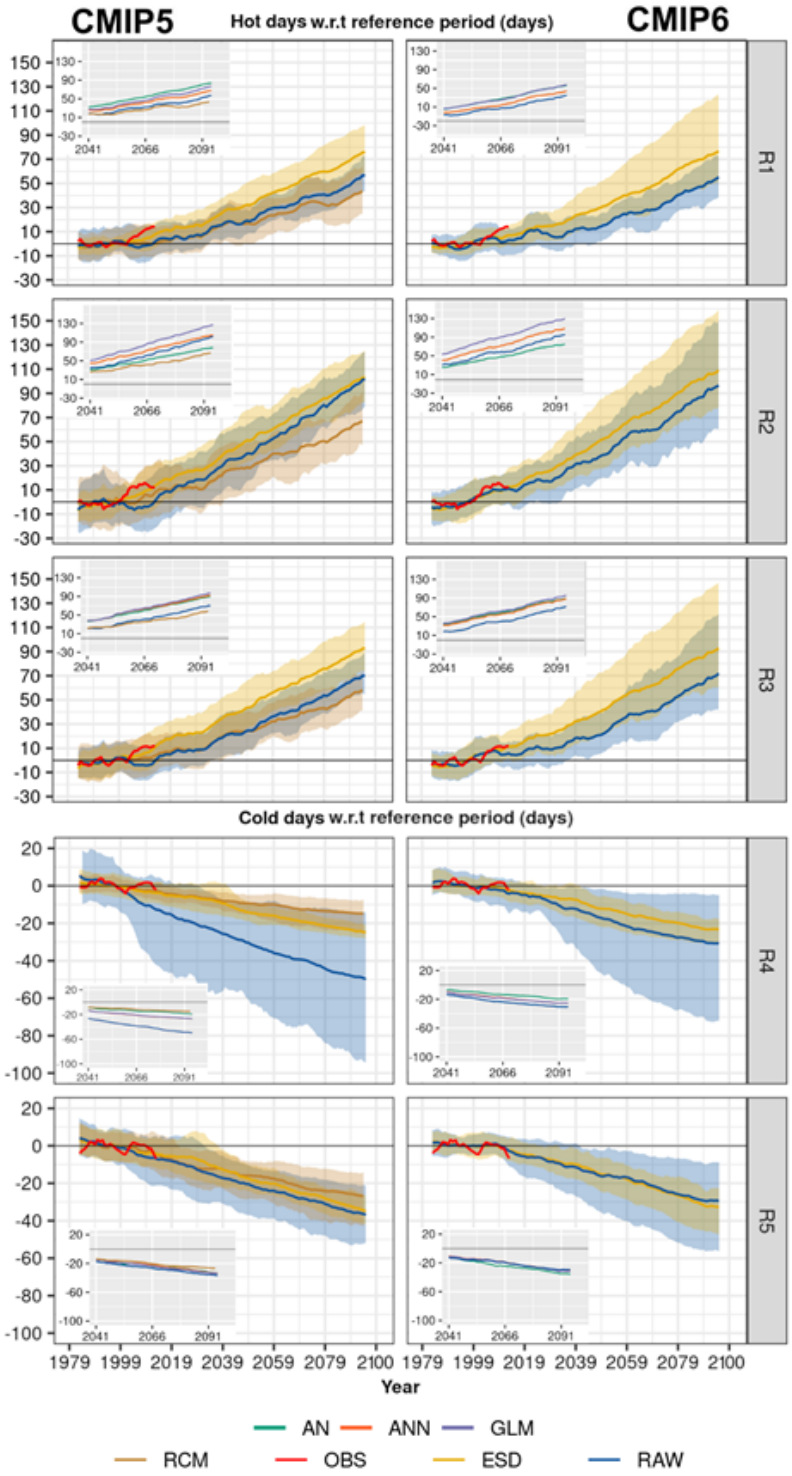

Figure 8

Regional time series of the indices warm days (in regions R1, R2 and R3) and cold days (in regions R4 and R5) for the ESD (yellow), RCMs (brown) and RAW (blue) simulations for the experiments CMIP5 and CMIP6. Observations are shown in red. In each case, the time evolution of the ESD simulations by the end of the century are shown in smaller figures, differentiated by set of statistical methods (ANs, GLMs, ANNs).

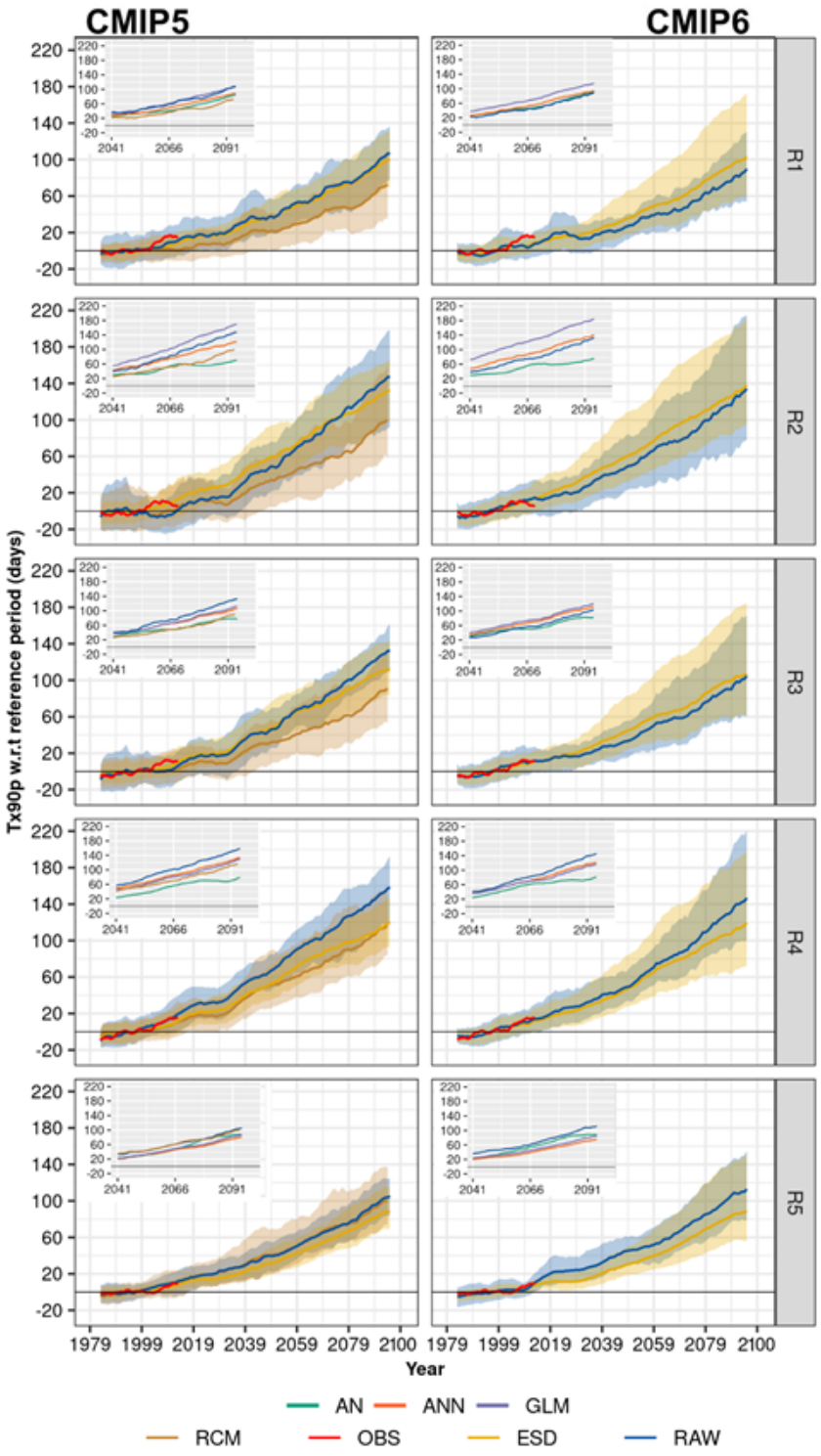

Figure 9

Similar to Figure 4 for Tx90p index.

Supplementary Files

This is a list of supplementary files associated with this preprint. Click to download.

- SupplementaryInformation.pdf